On the viability of detrital Rb-Sr geochronology

Kyle P. Larson[1], Brendan Dyck[1], Sudip Shrestha[2], Mark Button[2], Yani Najman[3]

[1]Department of Earth, Environmental and Geographic Sciences, University of British Columbia, Kelowna, V1V 1V7, Canada
[2]Fipke Laboratory for Trace Element Research, University of British Columbia, Kelowna, V1V 1V7, Canada
[3]Lancaster Environment Centre, Lancaster University, Lancaster, LA1 4YQ, UK

Correspondence to: Kyle P. Larson (kyle.larson@ubc.ca)

Abstract. Re-examination of sediment samples collected from the Bay of Bengal via laser-ablation inductively coupled plasma mass spectrometry (LA-ICP-MS) Rb-Sr geochronology demonstrates the viability of the Rb-Sr system for use as a detrital chronometer. The age population defined by the Rb-Sr dates essentially reproduces that previously published for detrital $^{40}Ar/^{39}Ar$ dates. The assumed initial $^{87}Sr/^{86}Sr$ on the calculated population has some influence on the age of the final population, but that influence can be ameliorated by filtering for higher $^{87}Rb/^{86}Sr$ ratios. The $^{87}Rb/^{86}Sr$ ratio cut-off used for such filters ~~to minimize the effect of initial $^{87}Sr/^{86}Sr$ on the final population~~ is strongly dependant on the age of the material being analysed (i.e. ~> $^{87}Rb/^{86}Sr$ = 500 @ 250 Ma and ~>$^{87}Rb/^{86}Sr$ = 50 @ 2500 Ma). Finally, Ti-in-biotite temperatures calculated based on data collected during LA-ICP-MS overlap with those calculated for the same material based on electron probe microanalyzer data demonstrating the potential for petrochronolgy based on the Rb-Sr system.

1 Introduction

Detrital geochronology is a commonly used approach to assess a wide variety of geological questions. For example, detrital zircon ~~age information~~ can provide information about the maximum depositional age for a sedimentary unit, likely sediment sources, and timescales of exhumation and sediment transport (e.g. Gehrels 2014; Thomas 2011; Malusà and Fitzgerald 2020). Moreover, detrital zircon chemistry can provide additional insight into the nature of the source rocks, such as crystallization depth and degree of fractional crystallization (e.g. Stevenson and Patchett 1990; Iizuka et al. 2010; Howard et al. 2009; Mueller et al. 2008). ~~Similarly~~, detrital ~~geochronology (often referred to as~~ thermochronology) ~~of mineral phases dated via radio-decay systems that may record cooling rather than crystallization,~~ such as $^{40}Ar/^{39}Ar$ on mica, or fission track and U-Th-He dating of U bearing minerals ~~is well suited~~ to quantify rates of exhumation and/or burial in active orogenic systems (e.g. Ruiz, Seward, and Winkler 2004; Najman et al. 1997, 2001).

Critical to detrital geochronology, in all forms, is analysing enough material to characterise the statistical variation in ~~the material being examined~~. Prior to the development of ~~spot~~ geochronology analytical techniques, analysing enough material (e.g. Vermeesch 2004) to characterise a specimen was time-consuming and expensive. The proliferation of laser ablation inductively coupled plasma mass spectrometry-based geochronology has enabled the rapid acquisition of large datasets.

While this is especially true for detrital U-Pb zircon geochronology, limitations still exist for other methods. For example, $^{40}Ar/^{39}Ar$ LA-ICP-MS geochronology still requires irradiation of samples prior to analyses, which increases the expense and time it takes to generate data.

The development of *in situ* beta decay geochronology techniques (e.g. Zack and Hogmalm 2016; Simpson et al. 2021) now allow additional detrital geochronometer options, with the critical caveat that these are typically isochron-based methods. As such, quantifying a non-radiogenic intercept is an integral part of calculating a date. In the absence of a measured cogenetic non-radiogenic phase to constrain that intercept, multiple radiogenic data points, which typically have varying initial isotopic reservoirs, can be regressed ~~through~~ to define a date. Such isochrons (regressions) rely on all analyses comprising a single closed isotopic system, which is incompatible with detrital geochronology. It is possible, however, to assume an initial, non-radiogenic intercept for isochron-based data and calculate two-point regressions through that intercept and each datapoint to calculate ~~an effective spot date.~~ For both Lu-Hf and Rb-Sr, the possible/expected initial ratios typically span a rather narrow range of values (e.g. 0.281-0.283 and 0.699-0.78; Rösel and Zack 2022; Fisher and Vervoort 2018). Moreover, the more radiogenic the spot analyses are, the less control the initial ratio exerts on the final two-point isochron date. This dependence is demonstrated in Larson et al. 2023, who show that correcting Rb-Sr data for common ^{87}Sr based on the current $^{87}Sr/^{88}Sr$, which effectively mimics the result of a two-point isochron through 0.71, effectively reproduces the isochron regression dates for samples with high Rb/Sr. The coincidence of the isochron and spot-dates derived independent of the measured initial $^{87}Sr/^{86}Sr$ indicates that detrital Rb-Sr geochronology may be a viable alternative or addition to detrital $^{40}Ar/^{39}Ar$ geochronology, eliminating the potential time-consuming step of irradiation.

This study presents the results of *in situ* Rb-Sr analysis of mica grains picked from sand samples collected from the Bay of Bengal that have either previously been dated via $^{40}Ar/^{39}Ar$ detrital geochronology or are directly adjacent to samples ~~that were~~ (see Najman et al. 2019). The potential viability of Rb-Sr as a detrital chronometer is compared against the published $^{40}Ar/^{39}Ar$ data. Moreover, the derivation of additional information (i.e., titanium-in-biotite temperature) from the mica grain via LA-ICP-MS is also investigated.

2 Methods

To test the viability of detrital U-Pb-Sr, samples (1450-24-25F; 1450-100-104-108F; 1451-47-49F, 1451-86F), collected from late Miocene to middle or late Pleistocene sediments during the Bengal Fan Ocean Discovery Program (IODP) Expedition 354, were examined. For simplicity, the sample names have been shortened here to 25F, 108F, 49F, and 86F, respectively. These same samples, or closely adjacent ones, have been previously investigated for detrital white mica $^{40}Ar/^{39}Ar$, zircon fission track, apatite U-Pb, and/or rutile U-Pb geochronology (Najman et al. 2019). Given the propensity for biotite (*sensu lato*) to be more radiogenic than white mica (e.g. Fournier, Camacho, and Lee 2016), and the sensitivity of low radiogenic material to the initial value of an isochron, biotite were targeted in this study. The biotite grains were either

manually picked from sediment separates and mounted in epoxy, or the sediments were poured directly into an epoxy mount. After polishing, biotite targets were verified via microXRF elemental mapping of each mount prior to analysis.

2.1 Rb-Sr geochronology

Rb-Sr geochronology was carried out via laser ablation inductively coupled plasma tandem mass spectrometry following the ~~basic~~ method set out in Zack and Hogmalm (2016) and Hogmalm et al. (Hogmalm et al. 2017) as described in Larson et al. (2023; 2023). Analyses were carried out in the Fipke Laboratory for Trace Element Research (FiLTER) at the University of British Columbia, Okanagan (UBCO) using an ESL NWR 193 laser with a TwoVol3 ablation cell paired with an Agilent 8900 triple quadruple (QQQ) ICP-MS. A circular laser spot, with a diameter of 65 microns, an estimated fluence of 3 J/cm^2 and repetition rate of 5 Hz was used for all unknowns and natural mica reference materials. Analyses of the glass reference material NIST610 (Jochum et al. 2011) were carried out using both 60 and 30 diameter laser spots to ensure analyses measured in both pulse and analogue detector modes for cross calibration (e.g. Zack and Hogmalm 2016). Instrument drift and down-hole fractionation was corrected based on analyses of NIST610 using an in-house data reduction scheme (Larson 2024) developed for Iolite v.4.8 (Paton et al. 2011). Matrix fractionation was corrected based on repeated analyses of Mica 1O (986 ± 5 Ma; Camacho et al. 2020) and verified based on the analyses of GA-1550 (Mt. Dromedary - 98.7 ± 1.9 Ma, Li et al. 2008). During run 1 (108F and 47-49F), GA-1550 returned an isochron date of 99.6 ± 3.5 Ma (mean squares weighted deviates (MSWD) = 1.9, n = 14/15, initial $^{87}Sr/^{86}Sr$ = 0.7049 ± 0.0017). During run 2 (25F and 86F), GA-1550 returned an isochron date of 98.1 ± 2.3 Ma (MSWD = 0.93, n = 17/17, initial $^{87}Sr/^{86}Sr$ = 0.7049 ± 0.0017) while an additional reference material, Mica 1B (990 ± 6 Ma; Camacho et al. 2012), returned an isochron date of 997 ± 6 Ma (MSWD = 3.7, n = 17/20, initial $^{87}Sr/^{86}Sr$ = 0.7035 ± 0.0005). Full Rb-Sr data are provided in Tables S1 and S2.

2.2 Ti-in-biotite thermometry

Titanium, magnesium, and iron contents for each Rb-Sr geochronology analytical spot were measured with the radiogenic ratios via LA-ICP-MS using 1 ms, 0.5 ms, and 1 ms dwell times, respectively. Concentrations were normalized to repeated measurements of the NIST610 glass reference material (Jochum et al. 2011) assuming stoichiometric Si (16.36 weight (wt.) % Si or 35 wt.% SiO_2), typical of metamorphic biotite from greenschist through granulite grade (e.g. Dyck et al. 2021). Titanium concentrations (ppm) were converted to molar weight per cation TiO_2 equivalents and then normalized to calculated Si content based on an assumed 5.4 atoms per formula unit (a.p.f.u.) Si per 22 O as detailed in Eq. (1):

(1) $Ti\ a.p.f.u = ({}_{C}Ti/{}_{WT}TiO_2/10000/{}_{M}TiO_2) * (5.4/{}_{A}Si)$

Where, ${}_{C}Ti$ = concentration of Ti in ppm, ${}_{WT}TiO2$ = weight proportion of Ti in TiO_2, ${}_{M}TiO_2$ = molar weight per cation, and ${}_{A}Si$ is the molar weight per cation Si assuming 35 wt % SiO_2. Ti-in-biotite temperatures were calculated using the equation of Henry et al. (2005), which requires Ti a.p.f.u and Mg# (=Mg/(Mg+Fe)) for each analysis. The values for Mg# were calculated using ppm concentrations of Fe and Mg. The 1σ uncertainty of the Ti-in-biotite temperatures is <24 °C at 480 °C decreasing to 12 °C at 800 °C (Henry, Guidotti, and Thomson 2005).

To verify the LA-ICP-MS derived Ti-in-biotite temperatures, the chemistries of the same mica grains were analysed using the Cameca SXFive FE electron probe microanalyser (EPMA) also housed in the FiLTER facility. Quantitative spot analyses were carried out with an acceleration voltage of 15kV, regulated beam current of 20nA and a spot size of 5um. Elemental x-ray data were collected using a dwell time of 30s on peak and 15s on background and were calibrated to the known composition of synthetic and natural mineral reference standards from Micro-Analysis Consultants Ltd. The EPMA data were converted to atoms per formula unit biotite on the basis of 22 oxygen whereby:

(2) cation (a.p.f.u.) = cation proportion * # oxygen (a.p.f.u.) / sum of oxygen proportions,

(3) oxygen proportion = cation proportion * (½) cation charge,

(4) cation proportion = oxide wt. % / oxide molecular wt.

Given that the biotite analysed was collected as detritus from the Bengal Fan, and the tendency of biotite to weather (e.g. Wilson 2004), alteration was expected. To avoid the most altered material, EPMA data were filtered for K concentrations > 1.1 a.p.f.u. Plotting K a.p.f.u against Mg# or calculated temperature shows that analyses with K a.p.f.u. > 1.1 rarely form outliers (Fig. 3). While it is recognized that an a.p.f.u of 1.1 K is significantly lower than that expected of unaltered biotite, K is expected to leave the mineral via hydrated cation exchange as part of the initial weathering stage/vermiculitization (Price and Velbel 2014; Gilkes and Suddhiprakarn 1979). In contrast, Fe, Mg and Ti are relatively immobile until more advanced alteration of biotite to geothite or kaolin (Gilkes and Suddhiprakarn 1979). Full EPMA data are provided in Table S3.

3 Results

3.1 Rb-Sr geochronology

All Rb-Sr results were filtered for Rb/Sr (>3), Fe + Mg (between 15 and 26 wt. %), and Ti (>0.1 a.p.f.u) to avoid spurious analyses. One hundred and thirty-two of 137 spot analyses of biotite from specimen 25F remained after filtering. The data spread between isochrons at 45 and 8 Ma and define an over-dispersed ca. 13 Ma isochron (Fig. 1A). Similarly, One-hundred and thirty-eight spots in biotite from 108F yield 102 viable analyses that spread between 5 and 30 Ma isochrons. The data define an over-dispersed isochron (MSWD = 5.5) at ca. 14 Ma (Fig. 1B). Ninety-six of 104 analyses in biotite separated from 49F spread between isochrons at 10 and 30 Ma, defining an over-dispersed (MSWD = 3.01) isochron at ca. 16 Ma (Fig. 1C). Finally, 113 of 117 biotite analyses of material from 86F spread between ~~reference~~ isochrons at 37 and 11 Ma and comprise an over-dispersed (MSWD = 6.88) isochron at ca. 15 Ma (Fig. 1D).

Spot dates for each analysis can be calculated in different ways: 1) two-point dates can be calculated based on a regression between each analysis and a specified initial $^{87}Sr/^{86}Sr$ value or 2) spot dates can be calculated based on the regression and intercept defined by the entire dataset as implemented in IsoplotR (Vermeesch 2018), calculation of the second method evaluates each analysis relative to the bulk regression removing a degree of freedom from the calculation relative to a two-point regression. Such a calculation results in smaller uncertainties and more limited variability in the resulting dates.

For each specimen, spot dates were calculated using both methods (see Tables S4-S7). For the two point regression method, dates were calculated assuming initial $^{87}Sr/^{86}Sr$ of 0.71, 0.72, 0.73, 0.74, 0.75 and 0.76, covering the range of expected values for most plutonic and metamorphic sources (Rösel and Zack 2022). The dates calculated for each specimen are provided in Table SX and depicted in Fig. 2 as kernel density estimations (KDE; bandwidth = 3). In general, the KDEs have a single peak for > 0 Ma dates (if a spot analysis has a $^{87}Sr/^{86}Sr$ < than the initial $^{87}Sr/^{86}Sr$, a negative date will be calculated, a situation exacerbated in young material that has not had time to accumulate radiogenic daughter product - see Table SX). The half-widths of the KDE peaks for each specimen are generally smallest for the dates calculated based on the isochron regressed through the bulk data and increase in width, decrease in height, and move to a younger position with two-point dates calculated with progressively higher initial $^{87}Sr/^{86}Sr$ (Fig. 2).

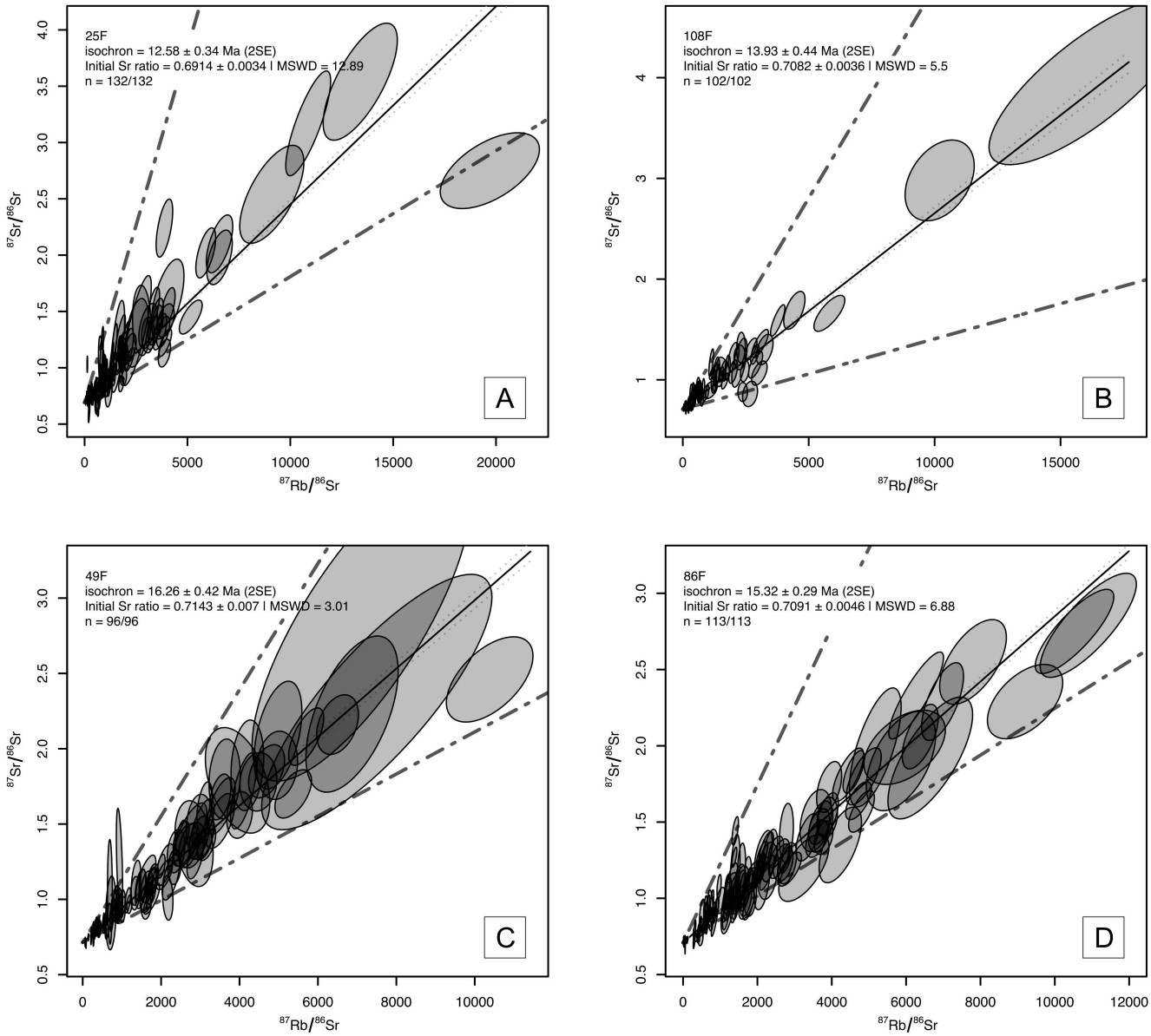

Figure 1: $^{87}Rb/^{86}Sr$ versus $^{87}Sr/^{86}Sr$ isochron plots of data collected from each sample investigated (A-D). Dashed grey lines denote the approximate envelope of each dataset with corresponding dates as marked. $^{40}Ar/^{39}Ar$ dates quoted are from Najman et al. (2019) and correspond to data from samples 1450-38-40F, 1450-98F, 1451-31-33-37F, and 1451-86F for 25F, 108F, 49F and 86F, respectively.

3.2 Ti-in-biotite thermometry

Ti-in-biotite temperatures calculated via LA-ICP-MS data generally range between ~ 650 and 725 ˚C for most samples (Fig. 3). While the precision of Ti data generated by LA-ICP-MS is lower than EPMA data, the second and third quartile temperatures overlap (within uncertainty) with those calculated using EPMA data for each specimen (Fig. 3).

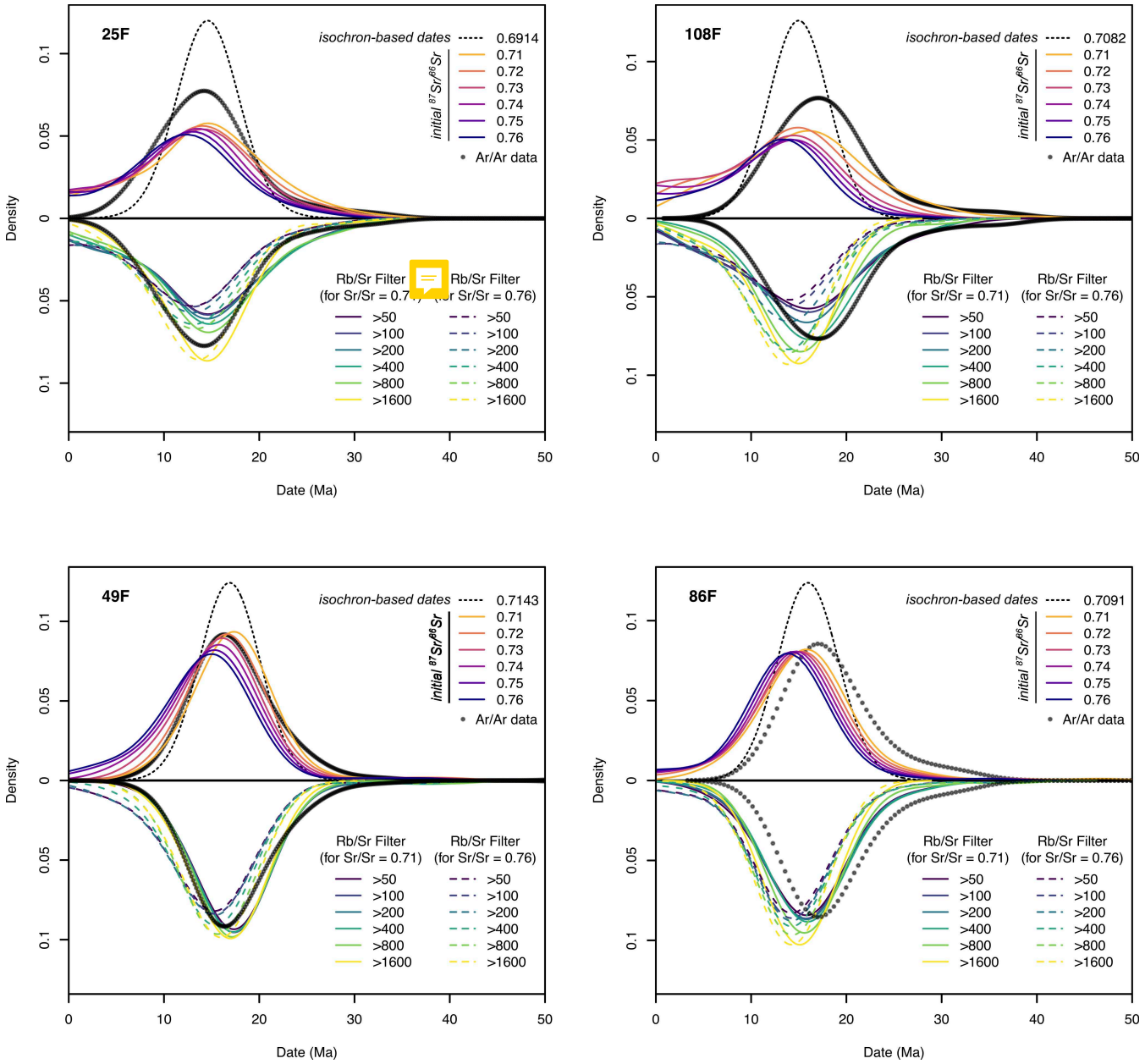

Figure 2: Kernel density estimation (KDE) plots of Rb-Sr data from samples analysed and $^{40}Ar/^{39}Ar$ of the same, or spatially adjacent, samples. The kernel bandwidth was 3 Ma for all plots. Each diagram shows two different datasets. The data plotted above the median line includes $^{40}Ar/^{39}Ar$ white mica dates and unfiltered Rb-Sr dates as marked. The 'isochron-based' dates are those calculated based on the bulk regression through the dataset, whereas the initial $^{87}Sr/^{86}Sr$ dates are calculated as two-point isochrons. Both types of dates were calculated using IsoplotR (Vermeesch, 2018). The data plotted below the median line represent the results of applying different $^{87}Rb/^{86}Sr$ filters, as noted.

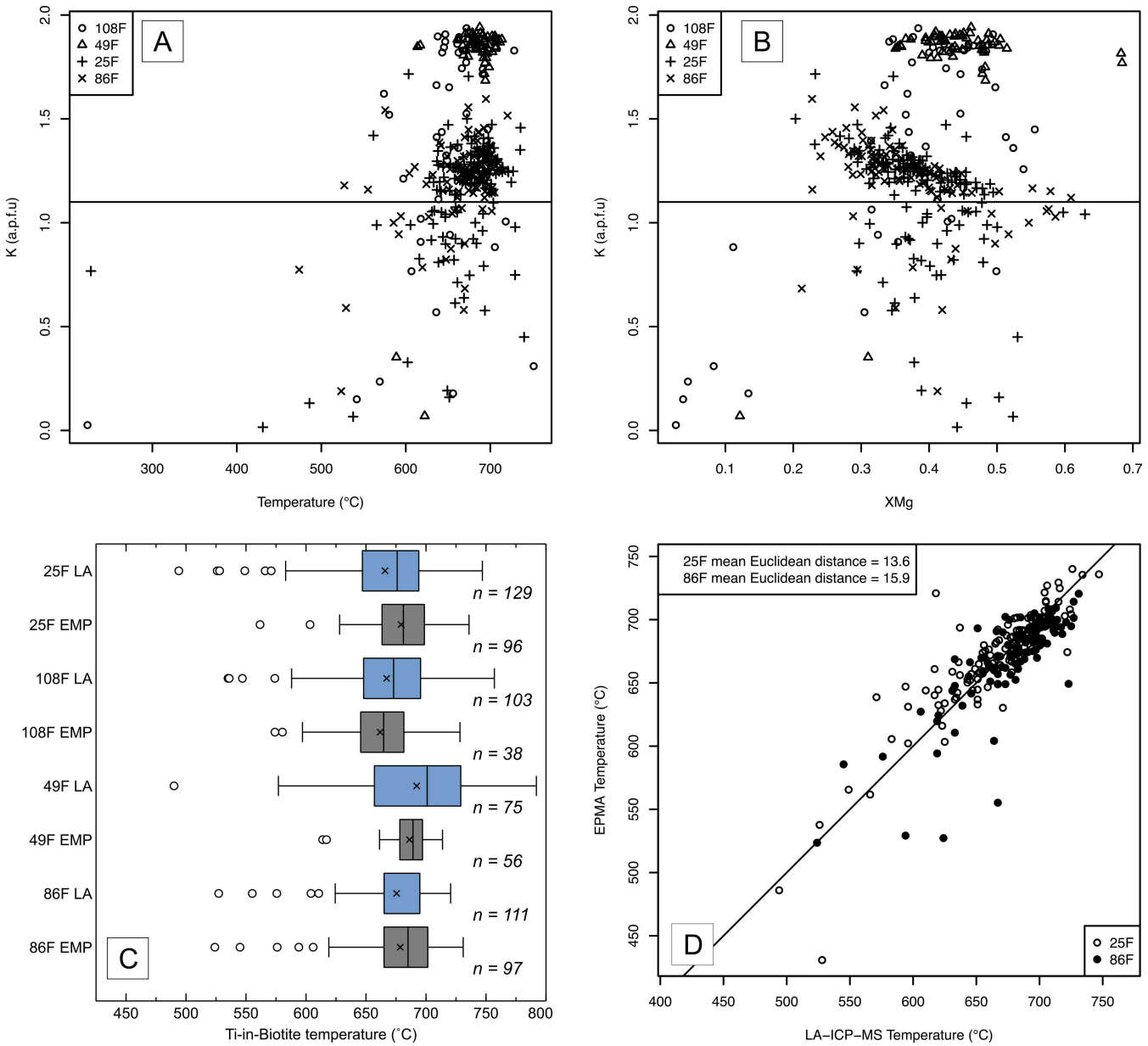

Figure 3: A) Plot of K atoms per formula unit (a.p.f.u; based on 22O) as calculated from electron probe microanalyser (EPMA) data versus derived Ti-in-biotite temperature. A horizontal line is drawn at K a.p.f.u = 1.1. B) Plot of K a.p.f.u. versus Mg# (Mg# = Mg/(Fe + Mg)) based on EPMA data. A horizontal line is drawn at K a.p.f.u = 1.1. C) Whisker and box plot of calculated Ti-in-biotite temperatures calculated for each sample via EPMA (grey fill) and laser ablation inductively coupled plasma mass spectrometer (LA-ICP-MS) data (blue fill). D) Plot of EPMA versus LA-ICP-MS temperatures for adjacent spot analyses on the same grains in samples 25F and 86F. Average Euclidean distance between the data points for each sample are shown.

4 Discussion

4.1 Effect of initial $^{87}Sr/^{86}Sr$

As with any isochron method, the value of the initial intercept can have a significant impact on the results when calculating two-point isochron Rb-Sr dates. That effect, however, is less significant with older material and more radiogenic analyses. As shown in Fig. 4, the effect of initial intercept can be demonstrated by generating three artificial datasets with 1 analysis every 500 $^{87}Rb/^{86}Sr$ spread between 10 and 4510, one defining a 25 Ma isochron, one defining a 250 Ma isochron and one defining a 2500 Ma isochron, each with an initial $^{87}Sr/^{86}Sr$ of 0.70. Two-point spot dates were calculated for each datapoint within each model for different initial $^{87}Sr/^{86}Sr$ ranging from 0.71 to 0.79 and the % change in two-point isochron date for each modelled point from the known date (i.e. 25, 250 or 2500 Ma) was quantified (Fig. 4). Plotting the % change in two-point isochron date versus $^{87}Rb/^{86}Sr$ demonstrates that low $^{87}Rb/^{86}Sr$ and young material is most affected by changing the initial $^{87}Sr/^{86}Sr$. Moreover, the plot further demonstrates that for high $^{87}Rb/^{86}Sr$ (>2500), even in young material, the typical difference in initial $^{87}Sr/^{86}Sr$ encountered in most crustal rocks (i.e. 0.70–0.76; Rösel and Zack 2022), will have < 5% effect on the date calculated (Fig. 4). For older material, the $^{87}Rb/^{86}Sr$ cut-offs to minimize the effect of initial $^{87}Sr/^{86}Sr$ on dates (i.e. < 5%) drops significantly (i.e. ~> $^{87}Rb/^{86}Sr$ = 500 @ 250 Ma and ~>$^{87}Rb/^{86}Sr$ = 50 @ 2500 Ma; Fig. 4).

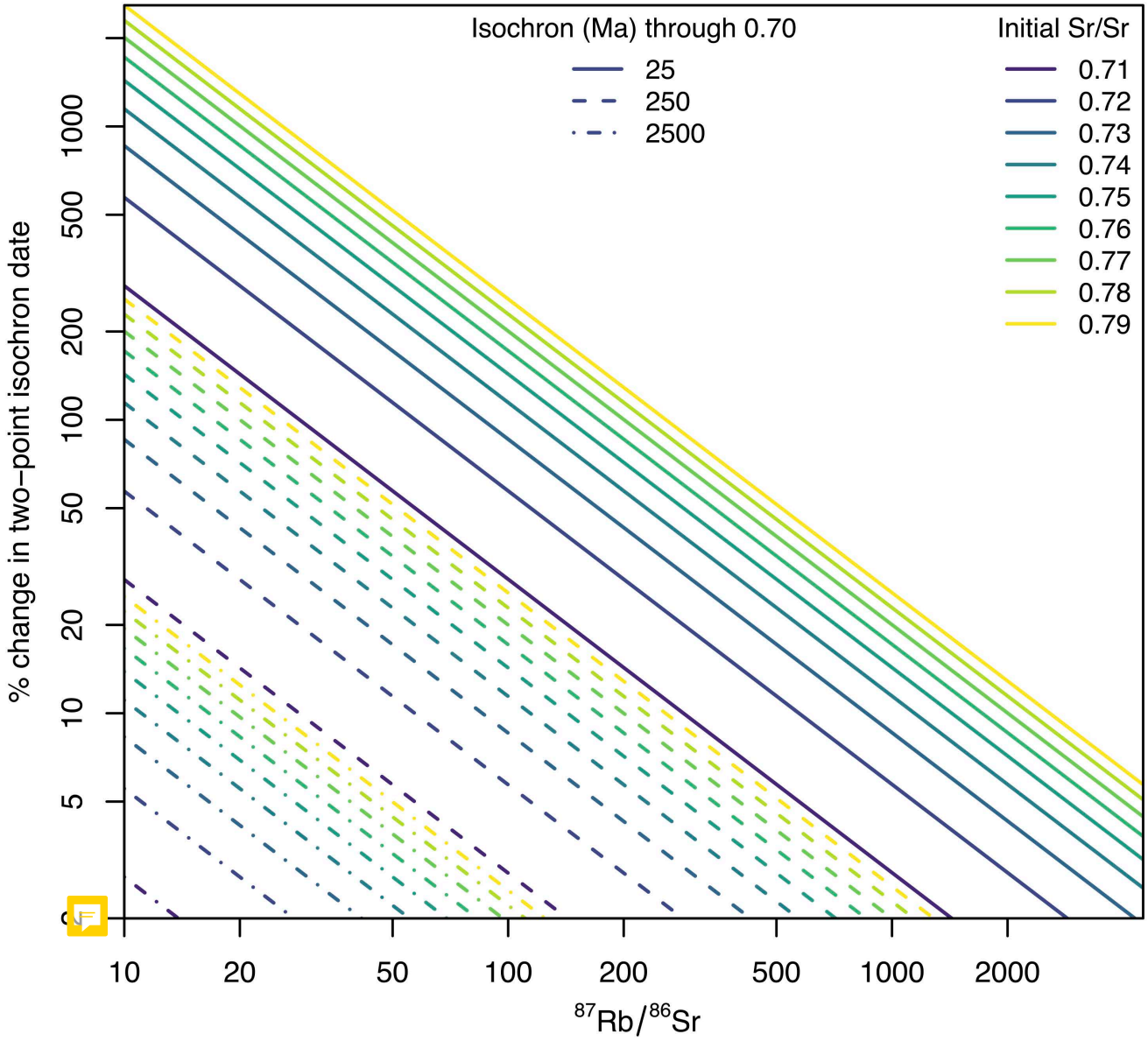

Figure 4: Plot of modelled data demonstrating the related effects of initial $^{87}Sr/^{86}Sr$ on calculated two-point isochron dates as a function of $^{87}Rb/^{86}Sr$. See text for discussion.

The effect of initial $^{87}Sr/^{86}Sr$ relative to $^{87}Rb/^{86}Sr$ can be further investigated using the real-world data presented herein. Filtering the two-point isochron dates based on $^{87}Rb/^{86}Sr$ for initial $^{87}Sr/^{86}Sr$ values of 0.71 and 0.76 demonstrates that the position of the main population of the data remains relatively invariant for each different $^{87}Rb/^{86}Sr$ but the half-width decreases and the density of the main population increases with higher $^{87}Rb/^{86}Sr$ cut-offs (Fig. 2). These results indicate that filtering detrital data by $^{87}Rb/^{86}Sr$ may help ameliorate the complication of unknown initial $^{87}Sr/^{86}Sr$ values.

4.2 Comparison with detrital $^{40}Ar/^{39}Ar$ geochronology

Najman et al. (2019) present the results of various detrital geochronology methods employed on the samples examined in the current study and/or other proximal samples. These methods include $^{40}Ar/^{39}Ar$ geochronology on white mica. White mica was targeted in that study both because of the common problem of excess Ar associated with biotite (Stübner et al. 2017; Larson, Button, et al. 2023) in the Himalayan system from which these samples were sampled (i.e. Himalayan detritus shed into the Bay of Bengal) and the resilience of white mica, relative to biotite, to weathering (Wilson 2004). Given the differences in clitid product retention between white mica $^{40}Ar/^{39}Ar$ geochronology and biotite Rb-Sr geochronology it may not be expected that the data from the two systems would overlap. White mica has an estimated nominal closure temperature of ~ 425-400 ˚C for Ar diffusion (100 micron radius grain, 10˚C/Ma cooling rate, 5-10 kbar; Harrison et al. 2009), whereas closure to diffusion of Sr out of biotite is more varied with estimates ranging from ~ 300 ˚C (Jager, Niggli, and Wenk 1967; Armstrong, Jäger, and Eberhardt 1966) to ~ 400 ˚C (Verschure et al. 1980; Del Moro et al. 1982) or even in >400 ˚C depending on the specifics of the mineralogy and chemistries of the samples (Jenkin et al. 1995, 2001). That variability in chronometer 'closure temperatures' (e.g. Dodson 1973) may be reflected in variable offsets between the Rb-Sr and $^{40}Ar/^{39}Ar$ dates (Fig. 2).

The two-point isochron and bulk regression-derived Rb-Sr dates calculated for 108F and 86F define a density peak with a slightly younger offset than the $^{40}Ar/^{39}Ar$ dates, whereas for 49F and 25F both types of dates essentially reproduce the density peak in the $^{40}Ar/^{39}Ar$ dates (Fig. 2). Overall, the Rb-Sr data, regardless of the method in which the dates were calculated, define the same dominant, early-middle Miocene age (15-16 Ma) population (Fig. 5) noted by Najman et al. (2019), which was interpreted to demonstrate rapid exhumation of the Eastern and Central Himalayan with a < 4 m.y. lag time between exhumation through mica closure to chlorite product diffusion and sedimentation. Given the similarities between the datasets, the detrital Rb-Sr geochronology would have led to the same conclusions as the $^{40}Ar/^{39}Ar$ data made by Najman et al. (2019).

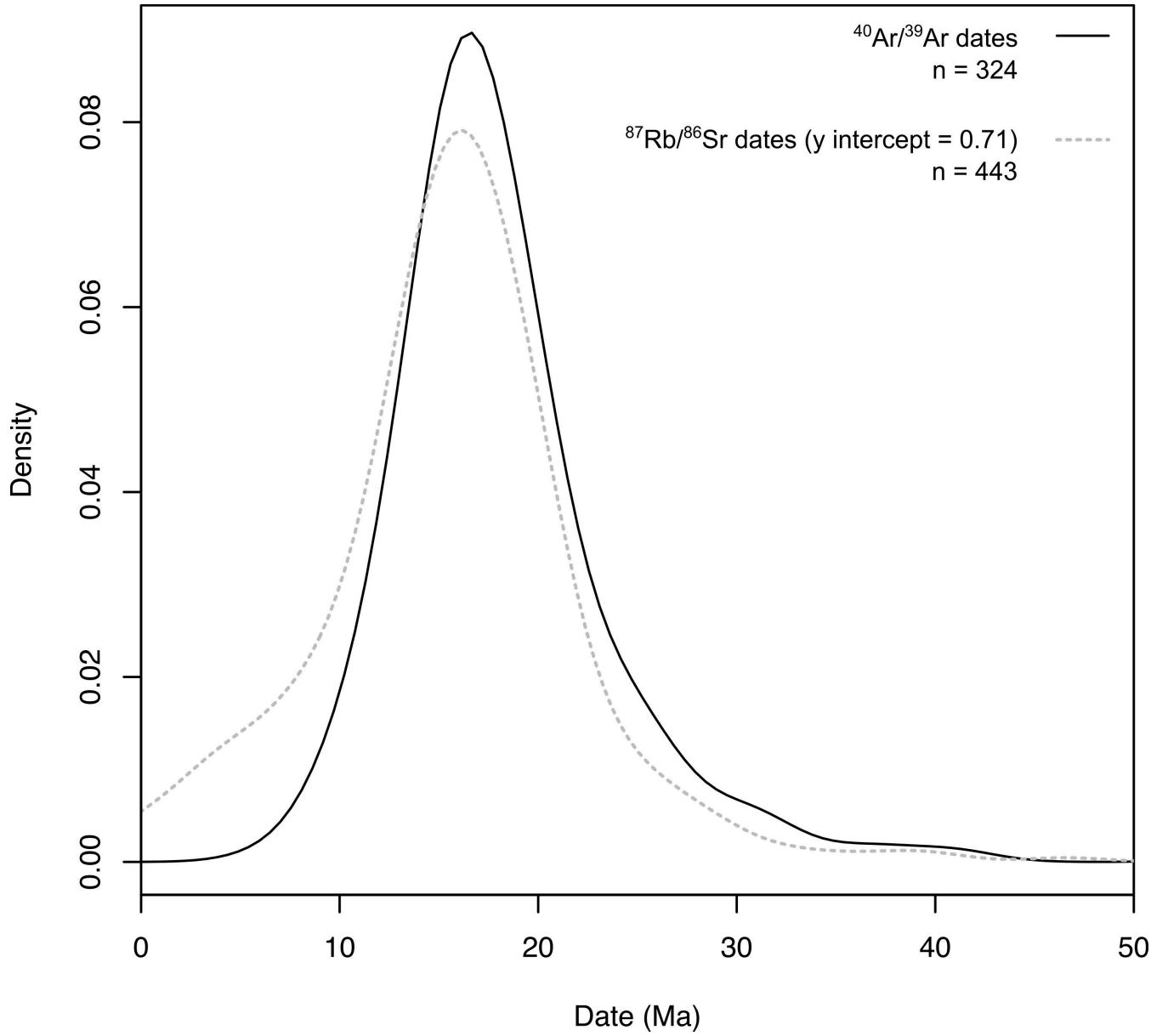

Figure 5: Kernel density estimations (bandwidth = 2) of all $^{40}Ar/^{39}Ar$ data reported by Najman et al. (2019) and all Rb-Sr spot-dates collected in the present study assuming an initial $^{87}Sr/^{86}Sr$ of 0.71.

4.3 Ti-in-biotite thermometry

Comparison of EPMA and LA-ICP-MS thermometry results demonstrate that LA-ICP-MS data can yield results comparable with traditional methods (Fig. 3). The temperatures calculated for the spot data are consistent with derivation from amphibolite-facies metamorphic rocks or associated leucogranites (e.g. Waters 2019), which dominate the inferred exhuming Himalayan midcrustal source (Najman et al. 2019). The temperatures also broadly overlap with Zr-in-rutile temperature

measured in detrital rutile from the same samples (Najman et al. 2019). Direct comparison of LA-ICP-MS and EPMA-derived temperatures for the same grains from 25F and 86F define mean Euclidean distances of 13.6 and 15.9 ˚C, respectively (Fig. 3). Because this approximately 15 °C uncertainty likely reflects the analytical precision of LA-ICP-MS rather than solely due to the uncertainties stemming from natural variations in biotite chemistry nor the thermometer calibration, it should be considered additive to the ±12–24 °C 1σ uncertainty of Henry et al., (2005). The precision on the Ti-in-biotite temperature estimates, whether EPMA or LA-ICP-MS derived, does not facilitate quantifying a change across the sampled strata; data from all samples overlap (Fig.3).

The viability of quantifying Ti-in-biotite temperatures via LA-ICP-MS allows each Rb-Sr spot analysed to be associated with a unique temperature. This kind of petrochronologic association opens the possibility of many different types of studies, not unlike the linking of chemistry to spot dates did for U(-Th)-Pb geochronology in the early 2000s (e.g. Foster et al. 2004; Gibson et al. 2004; Rubatto 2002).

5 Conclusions

LA-ICP-MS Rb-Sr geochronology appears to be a viable method to efficiently generate detrital biotite geochronological datasets. The effect of unknown initial $^{87}Sr/^{86}Sr$ values can be mitigated for young (Cenozoic) material by filtering for significantly radiogenic analyses ($^{87}Rb/^{86}Sr$ > 2000). Filtering can be less aggressive for older material (i.e. >500 @ 250 Ma) in which significant radiogenic child product has accumulated. Finally, the benefits of biotite Rb-Sr geochronology can be further extended by calculating a Ti-in-biotite temperature for each spot. Such information may allow for identification of multiple sources in detrital samples with complex provenance.

Data availability

All data related to this study are available on the Open Science Framework website: https://osf.io/vgjh6/?view_only=52b27e0d000c4f2ea6b9ab665744e43c

Author contributions

KPL – conceptualization; funding acquisition, methodology, investigation, visualization, writing – original draft preparation; BD – methodology, investigation, writing – review and editing; SS – investigation, writing – review and editing; MB – investigation, writing – review and editing; YN – resources, writing – review and editing.

Competing interests

None of the authors have any competing interests.

Financial Support

This study was supported by a Natural Science and Engineering Research Council of Canada Discovery Grant to K. Larson.

References

Armstrong, Richard L., Emilie Jäger, and Peter Eberhardt. 1966. "A Comparison of K-Ar and Rb-Sr Ages on Alpine Biotites." *Earth and Planetary Science Letters* 1 (1): 13–19.

Camacho, A., J. K. W. Lee, J. D. Fitz Gerald, J. Zhao, Y. A. Abdu, D. M. Jenkins, F. C. Hawthorne, et al. 2012. "Planar Defects as Ar Traps in Trioctahedral Micas: A Mechanism for Increased Ar Retentivity in Phlogopite." *Earth and Planetary Science Letters* 341–344 (August): 255–67.

Camacho, A., J. K. W. Lee, J. Zhao, Y. A. Abdu, M. Fayek, and R. A. Creaser. 2020. "A Test of the Interlayer Ionic Porosity Model as a Measure of Argon Diffusivity in Trioctahedral Micas." *Geochimica et Cosmochimica Acta* 288 (November): 341–68.

Del Moro, A., M. Puxeddu, F. Radicati di Brozolo, and I. M. Villa. 1982. "Rb-Sr and K-Ar Ages on Minerals at Temperatures of 300°–400° C from Deep Wells in the Larderello Geothermal Field (Italy)." *Contributions to Mineralogy and Petrology. Beitrage Zur Mineralogie Und Petrologie* 81 (4): 340–49.

Dodson, Martin. 1973. "Closure Temperature in Cooling Geochronological and Petrological Systems." *Contributions to Mineralogy and Petrology* 40 (January): 259–74.

Dyck, Brendan, Rellie M. Goddard, David Wallis, Lars N. Hansen, and Edith Martel. 2021. "Metamorphic Evolution of the Great Slave Lake Shear Zone." *Journal of Metamorphic Geology* 39 (5): 567–90.

Fisher, Christopher M., and Jeffrey D. Vervoort. 2018. "Using the Magmatic Record to Constrain the Growth of Continental Crust—The Eoarchean Zircon Hf Record of Greenland." *Earth and Planetary Science Letters* 488 (April): 79–91.

Foster, Gavin L., Randall R. Parrish, Matthew S. A. Horstwood, S. Chenery, J. Pyle, and H. Daniel Gibson. 2004. "The Generation of Prograde P–T–t Points and Paths; a Textural, Compositional, and Chronological Study of Metamorphic Monazite." *Earth and Planetary Science Letters* 228 (1–2): 125–42.

Fournier, H. W., A. Camacho, and J. K. W. Lee. 2016. "High-Strain Deformation and Fluid Infiltration Diachronism of the Middle Crust: New Devonian–Permian Alice Springs Ages (365–290 Ma) of Shear Zones in the Strangways Metamorphic Complex, Central Australia." *Chemical Geology* 443: 39–53.

Gehrels, George. 2014. "Detrital Zircon U-Pb Geochronology Applied to Tectonics." *Annual Review of Earth and Planetary Sciences* 42 (1): 127–49.

Gibson, H. Daniel, Sharon D. Carr, Richard L. Brown, and Michael A. Hamilton. 2004. "Correlations between Chemical and Age Domains in Monazite, and Metamorphic Reactions Involving Major Pelitic Phases: An Integration of ID-TIMS and SHRIMP Geochronology with Y–Th–U X-Ray Mapping." *Chemical Geology* 211 (January): 237–60.

Gilkes, R. J., and Anchalee Suddhiprakarn. 1979. "Biotite Alteration in Deeply Weathered Granite. I. Morphological, Mineralogical, and Chemical Properties." *Clays and Clay Minerals* 27 (5): 349–60.

Harrison, T. Mark, Julien Célérier, Amos B. Aikman, Joerg Hermann, and Matthew T. Heizler. 2009. "Diffusion of ^{40}Ar in Muscovite." *Geochimica et Cosmochimica Acta* 73 (4): 1039–51.

Henry, Darrell J., Charles V. Guidotti, and Jennifer A. Thomson. 2005. "The Ti-Saturation Surface for Low-to-Medium Pressure Metapelitic Biotites: Implications for Geothermometry and Ti-Substitution Mechanisms." *The American Mineralogist* 90 (2–3): 316–28.

Hogmalm, J. K., Thomas Zack, Andreas K. -O. Karlsson, Axel S. L. Sjöqvist, and Dieter Garbe-Schönberg. 2017. "In Situ Rb–Sr and K–Ca Dating by LA-ICP-MS/MS: An Evaluation of N_2O and SF_6 as Reaction Gases." *Journal of Analytical Atomic Spectrometry* 32 (2): 305–13.

Howard, Katherine E., Martin Hand, Karin M. Barovich, Anthony Reid, Benjamin P. Wade, and Elena A. Belousova. 2009. "Detrital Zircon Ages: Improving Interpretation via Nd and Hf Isotopic Data." *Chemical Geology* 262 (3): 277–92.

Iizuka, Tsuyoshi, Tsuyoshi Komiya, Shuji Rino, Shigenori Maruyama, and Takafumi Hirata. 2010. "Detrital Zircon Evidence for Hf Isotopic Evolution of Granitoid Crust and Continental Growth." *Geochimica et Cosmochimica Acta* 74 (8): 2450–72.

Jager, Emilie, Ernst Niggli, and Eduard Wenk. 1967. *Rb-Sr Altersbestimmungen an Glimmern Der Zentralalpen*. Kummerly & Frey.

Jenkin, Gawen R. T., Robert M. Ellam, Graeme Rogers, and Finlay M. Stuart. 2001. "An Investigation of Closure Temperature of the Biotite Rb-Sr System: The Importance of Cation Exchange." *Geochimica et Cosmochimica Acta* 65 (7): 1141–60.

Jenkin, Gawen R. T., Graeme Rogers, Anthony E. Fallick, and Colin M. Farrow. 1995. "Rb-Sr Closure Temperatures in Bi-Mineralic Rocks: A Mode Effect and Test for Different Diffusion Models." *Chemical Geology* 122 (1–4): 227–40.

Jochum, Klaus Peter, Ulrike Weis, Brigitte Stoll, Dmitry Kuzmin, Qichao Yang, Ingrid Raczek, Dorrit E. Jacob, et al. 2011. "Determination of Reference Values for NIST SRM 610-617 Glasses Following ISO Guidelines." *Geostandards and Geoanalytical Research* 35 (4): 397–429.

Larson, Kyle P. 2024. *LA-ICP-MS RbSr Data Reduction Scheme*. OSF. https://doi.org/10.17605/OSF.IO/VJAF2.

Larson, Kyle P., Mark Button, Sudip Shrestha, and Alfredo Camacho. 2023. "A Comparison of $^{87}Rb/^{87}Sr$ and $^{40}Ar/^{39}Ar$ Dates: Evaluating the Problem of Excess ^{40}Ar in Himalayan Mica." *Earth and Planetary Science Letters* 609 (May): 118058.

Larson, Kyle P., Brendan Dyck, Shah Faisal, John M. Cottle, and Mike Searle. 2023. "Metamorphic and Intrusive History of the Hindu Raj Region, Northern Pakistan." *Geological Magazine* 160 (7): 1376–94.

Li, Qiu-Li, Fukun Chen, Xiang-Hui Li, Fei Wang, and Huai-Yu He. 2008. "Single Grain Rb-Sr Isotopic Analysis of GA-1550 Biotite, LP-6 Biotite and Bern-4M Muscovite 40Ar-39Ar Dating Standards." *Geochemical Journal* 42 (3): 263–71.

Malusà, Marco G., and Paul G. Fitzgerald. 2020. "The Geologic Interpretation of the Detrital Thermochronology Record within a Stratigraphic Framework, with Examples from the European Alps, Taiwan and the Himalayas." *Earth-Science Reviews* 201 (February): 103074.

Mueller, Paul A., George D. Kamenov, Ann L. Heatherington, and Joshua Richards. 2008. "Crustal Evolution in the Southern Appalachian Orogen: Evidence from Hf Isotopes in Detrital Zircons." *The Journal of Geology* 116 (4): 414–22.

Najman, Yani, Chris Mark, Dan N. Barfod, Andy Carter, Randy Parrish, David Chew, and Lorenzo Gemignani. 2019. "Spatial and Temporal Trends in Exhumation of the Eastern Himalaya and Syntaxis as Determined from a Multitechnique Detrital Thermochronological Study of the Bengal Fan." *GSA Bulletin* 131 (9–10): 1607–22.

Najman, Yani, M. S. Pringle, Laurent Godin, and Grahame Oliver. 2001. "Dating of the Oldest Continental Sediments from the Himalayan Foreland Basin." *Nature* 410 (March): 194–97.

Najman, Yani, M. S. Pringle, Michael Johnson, A. H. F. Robertson, and J. R. Wijbrans. 1997. "Laser $^{40}Ar/^{39}Ar$ Dating of Single Detrital Muscovite Grains from Early Foreland-Basin Sedimentary Deposits in India: Implications for Early Himalayan Evolution." *Geology* 25 (6): 535–38.

Paton, Chad, John Hellstrom, Bence Paul, Jon Woodhead, and Janet Hergt. 2011. "Iolite: Freeware for the Visualisation and Processing of Mass Spectrometric Data." *Journal of Analytical Atomic Spectrometry* 26 (12): 2508–12.

Price, Jason R., and Michael A. Velbel. 2014. "Rates of Biotite Weathering, and Clay Mineral Transformation and Neoformation, Determined from Watershed Geochemical Mass-Balance Methods for the Coweeta Hydrologic Laboratory, Southern Blue Ridge Mountains, North Carolina, USA." *Aquatic Geochemistry* 20 (2–3): 203–24.

Rösel, Delia, and Thomas Zack. 2022. "LA-ICP-MS/MS Single-spot Rb-Sr Dating." *Geostandards and Geoanalytical Research* 46 (2): 143–68.

Rubatto, Daniela. 2002. "Zircon Trace Element Geochemistry: Partitioning with Garnet and the Link between U–Pb Ages and Metamorphism." *Chemical Geology* 184 (1): 123–38.

Ruiz, G. M. H., D. Seward, and W. Winkler. 2004. "Detrital Thermochronology - a New Perspective on Hinterland Tectonics, an Example from the Andean Amazon Basin, Ecuador." *Basin Research* 16 (3): 413–30.

Simpson, Alexander, Sarah Gilbert, Renee Tamblyn, Martin Hand, Carl Spandler, Jack Gillespie, Angus Nixon, and Stijn Glorie. 2021. "In-Situ Lu-Hf Geochronology of Garnet, Apatite and Xenotime by LA ICP MS/MS." *Chemical Geology* 577 (September): 120299.

Stevenson, Ross K., and P. Jonathan Patchett. 1990. "Implications for the Evolution of Continental Crust from Hf Isotope Systematics of Archean Detrital Zircons." *Geochimica et Cosmochimica Acta* 54 (6): 1683–97.

Stübner, Konstanze, Clare Warren, Lothar Ratschbacher, Blanka Sperner, Reinhard Kleeberg, Jörg Pfänder, and Djordje Grujic. 2017. "Anomalously Old Biotite $^{40}Ar/^{39}Ar$ Ages in the NW Himalaya." *Lithosphere* 9 (3): 366–83.

Thomas, William A. 2011. "Detrital-Zircon Geochronology and Sedimentary Provenance." *Lithosphere* 3 (4): 304–8.

Vermeesch, Pieter. 2004. "How Many Grains Are Needed for a Provenance Study?" *Earth and Planetary Science Letters* 224 (3): 441–51.

———. 2018. "IsoplotR: A Free and Open Toolbox for Geochronology." *Geoscience Frontiers* 9 (5): 1479–93.

Verschure, R. H., P. A. M. Andriessen, N. A. I. M. Boelrijk, E. H. Hebeda, C. Maijer, H. N. A. Priem, and E. A. Th Verdurmen. 1980. "On the Thermal Stability of Rb-Sr and K-Ar Biotite Systems: Evidence from Coexisting Sveconorwegian (ca 870 Ma) and Caledonian (ca 400 Ma) Biotites in SW Norway." *Contributions to Mineralogy and Petrology. Beitrage Zur Mineralogie Und Petrologie* 74 (3): 245–52.

Waters, David John. 2019. "Metamorphic Constraints on the Tectonic Evolution of the High Himalaya in Nepal: The Art of the Possible." *Geological Society, London, Special Publications* 483 (January): SP483-2018–2187.

Wilson, M. J. 2004. "Weathering of the Primary Rock-Forming Minerals: Processes, Products and Rates." *Clay Minerals* 39 (3): 233–66.

Zack, Thomas, and K. Johan Hogmalm. 2016. "Laser Ablation Rb/Sr Dating by Online Chemical Separation of Rb and Sr in an Oxygen-Filled Reaction Cell." *Chemical Geology* 437 (October): 120–33.